Available online at www.sciencedirect.com
ScienceDirect
Journal of Crystal Growth 300 (2007) 353–357
JOURNAL OF CRYSTAL GROWTH
www.elsevier.com/locate/jcrysgro

Effect of grain size on the electrical properties of ultraviolet photodetector with ZnO/diamond film structure

Jian Min Liu[a,b,*], Yi Ben Xia[a], Lin Jun Wang[a], Qing Feng Su[a], Wei Min Shi[a]

[a]*School of Materials Science and Engineering, 149 yanchang Road, Shanghai University, Shanghai 200072, China*
[b]*Jingdezhen Ceramic Institute, Jingdezhen Jiangxi 333001, China*

Received 31 July 2006; received in revised form 23 October 2006; accepted 15 December 2006
Communicated by M. Kawasaki
Available online 14 January 2007

Abstract

Highly *c*-axis-oriented ZnO films were successfully deposited on the nucleation sides of freestanding diamond films by RF reactive magnetron sputtering. *I–V* characteristics of ultraviolet (UV) photodetectors with ZnO/diamond structure were studied and a significant photoresponse was observed under UV light illumination. The dark-current and the photocurrent of the ZnO photodetectors were relative to the grain size and the quality of ZnO films. For the photodetector with a bigger grain size, a weaker dark current and a stronger photocurrent were obtained under 10 V bias voltage. The photocurrent rise and decay process confirmed the carrier-trapping effect.

PACS: 81.05.Dz; 61.80.Ba; 72.40.+w

Keywords: A1. Grain size; A1. Photoresponse; B1. Diamond; B1. ZnO; B3. Photodetector

1. Introduction

Modern high-power electronic devices suffer severe cooling problems due to the production of large amounts of heat in a small area. In order to cool these devices, it is essential to spread the narrow heat flux by placing a layer of high thermal conductivity between the device and the cooling system [1]. Due to the highest thermal conductivity, wide band gap, high radiation resistance, good chemical and temperature stability, diamond is presumed to be an ideal heat exchange material (heat sink and heat spreader), which can be used at high temperature, high flux and in severe environments [2–4].

ZnO, one of the most important II–VI group semiconductors, presents many remarkable characteristics due to its large bond strength, good optical quality, extreme stability of excitons and excellent piezoelectric properties [5]. Another advantage of ZnO relative to other materials is its low price, non-toxicity and relatively low deposition temperature. Therefore, ZnO is attracting attention for its extensive applications for surface acoustic wave (SAW) devices, gas sensors, transparent conducting layers, light-emitting diodes (LEDs), ultraviolet (UV) lasers and especially the UV detectors [6–8]. ZnO UV detectors have many of the important applications for satellite-based missile plume detection, in situ combustion monitoring gas, air quality monitoring, gas sensing, accurate measurement of radiation for the treatment of UV-irradiated skin, etc. [9].

In this paper, we try to use diamond as the substrate of the ZnO electronic device. The application of the diamond film is expected to improve the performance of ZnO UV detectors for high-temperature and high-power electronic applications. In our work, the highly *c*-axis-oriented ZnO films with different grain size and quality are deposited on the freestanding diamond films. And then metal–semiconductor–metal (MSM) structural UV photodetectors are

*Corresponding author. Tel.: +86 02156331715; fax: +86 02156332694.
E-mail address: liujianmin66@126.com (J.M. Liu).

0022-0248/$ - see front matter © 2007 Elsevier B.V. All rights reserved.
doi:10.1016/j.jcrysgro.2006.12.029

fabricated on diamond substrates and their photoresponse characteristics and grain size effects are investigated.

2. Experimental details

Freestanding diamond film was prepared on mirror-polished n-type (1 0 0) silicon wafer. The thickness is about 80 μm. The detailed process was introduced elsewhere [10].

ZnO films were attempted to deposit on the nucleation sides of freestanding diamond films by RF frequency magnetron sputtering. The air pressure in reaction chamber was pumped down to 3×10^{-3} Pa prior to the introduction of argon (99.999%) and oxygen (99.999%). The sputtering conditions were as follows: sputtering power: 400 W, the rate of argon and oxygen: 7:1, gas pressure: 0.6 Pa; substrate temperature: room temperature, time: 1 h, 2 h (for samples a and b) and target material: ZnO ceramic (99.99%).

Au circle electrode contacts ($r = 0.5$ mm) on the film surface were formed by the DC magnetron sputtering, the interval of contacts was 2 mm. Then, the sample was annealed at 400 °C in the air for 1 h in order to make ohmic metal alloying.

Related characteristics of the films were analyzed by scanning electron microscope (SEM JSM-6700F), atomic force microscope (AFM AP-0190), Raman spectroscopy (RH-800 type) and X-ray diffraction (XRD D/MAX-3C) and HP 4192A impedance analyzer. A 150 W xenon lamp connected with a monochromator (Photon Technology International, Model 101) was used As UV light sources. The detector was placed on the monochromator's exit slit with a distance of 2 cm in air at room temperature and its current was measured by the a KEITHLEY 4200SCS semiconductor characterization system. The wavelength of incidence used in our experiments is 320 nm.

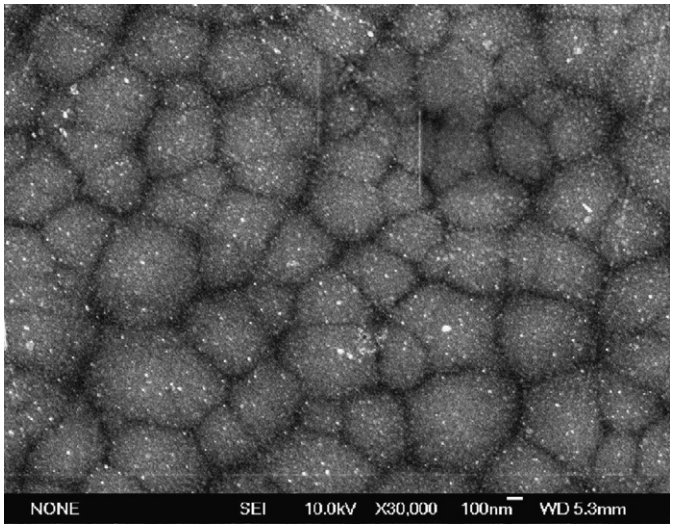

Fig. 1. A typical SEM image for the nucleation side of freestanding diamond film.

3. Results and discussion

A typical SEM image of the nucleation side of free-standing diamond film is shown in Fig. 1, from which it can be seen that nucleation side is very smooth. The surface roughness of the nucleation side is about 1.5 nm (1 μm × 1 μm) observed by AFM measurements.

The Raman spectrum for the diamond film is shown in Fig. 2. A strong Raman scattering peak of diamond exists at about 1334 cm^{-1} and a weak Raman scattering peak of non-diamond carbon exists at about 1550 cm^{-1}. By considering that the sensitivity of the Raman signal for the non-diamond carbon phase is about 75 times that for diamond, Raman spectroscopy is also used to estimate the non-diamond carbon content (C_{nd}) [11]

$$C_{nd} = 1/[1 + 75(I_d/I_{nd})], \quad (1)$$

where I_d is Raman peak intensity for diamond crystals and I_{nd} is Raman peak intensity for non-diamond carbon phase. It is concluded that the content of non-diamond carbon is low, which shows high quality for freestanding diamond film.

The frequency dependence of dielectric properties of the diamond substrate is very important for high-frequency electronic applications. The room temperature frequency dependence of dielectric constant and dielectric loss of freestanding diamond film is shown in Fig. 3. The dielectric constant of diamond films can be expressed as

$$\varepsilon = Cd/\varepsilon_0 S, \quad (2)$$

where d is the film thickness, S the area of contact and ε_0 the permittivity of free space.

It can be seen that the dielectric constant and dielectric loss decrease with increase of frequency and it is saturated at higher frequency (the dielectric constant 7.78, dielectric loss 0.07 at 10 MHz). An increase of the dielectric constant at low frequencies can attribute to low-frequency dispersion (LFD) [12,13]. This phenomenon is present in the dielectric spectra as a strong increase, thus increasing the

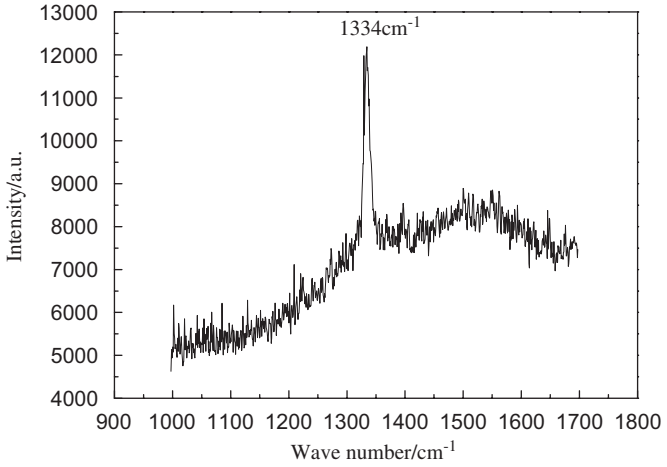

Fig. 2. Raman spectrum for the freestanding diamond film.

dielectric loss. LFD could be associated with the loss in the boundaries of the crystals. This dielectric loss may be produced by different processes such as the intercrystalline border barrier potential or a larger defect density in diamond and amorphous carbon. All these processes are not exclusive, because they are determined by the polycrystalline nature of CVD diamond films and present in the films at the same time.

Fig. 4 exhibits AFM images of the ZnO films deposited for different sputtering times. As can be seen from Fig. 2, the ZnO films have a compact, dense and uniform structure, with the crystallite dimension normal to the c-axis of about 40 and 100 nm. AFM measurements show the surface roughness of ZnO film is about 3.4 and 8.2 nm (1 μm × 1 μm), respectively.

XRD pattern for ZnO/freestanding diamond films is shown in Fig. 5, which exhibits diamond (1 1 1) peak and preferential-oriented ZnO (0 0 2) peak. The intensity of ZnO (0 0 2) peak increases with the increase of sputtering time. The full-width at half-maximum (FWHM) of ZnO (0 0 2) peak is about 0.36° at 34.26° and 0.30° at 34.46° for sample a and b, respectively. The crystallite sizes are also calculated from the FWHM of the XRD spectra by using the relationship [14]

$$D = 0.9\lambda/\omega \cos\theta, \tag{3}$$

where λ is the diffractometer wavelength, ω the FWHM and θ the diffraction angle of the XRD spectra. According to the formula, we can conclude that with the increase of sputtering time, the crystallite size and quality of ZnO films increase. The results of XRD are consistent with those of AFM.

Fig. 6 shows the dark-current and photocurrent characteristics as a function of bias voltage for ZnO/diamond film structure photodetectors. The dark-current and photocurrent voltage characteristics appear nearly symmetric and linear both in respect to current and voltage inversion, indicating that a fine ohmic contact is formed for bias voltage up to 10 V. The photocurrent almost proportionally increases with voltage, due to the proportionally linear relationship between the collected carriers and external electrical field, conformed to a simple photogeneration and collection model [15] where the photocurrent can be written as

$$I_{ph} = qF_0\eta_{abs}\mu\tau E/d, \tag{4}$$

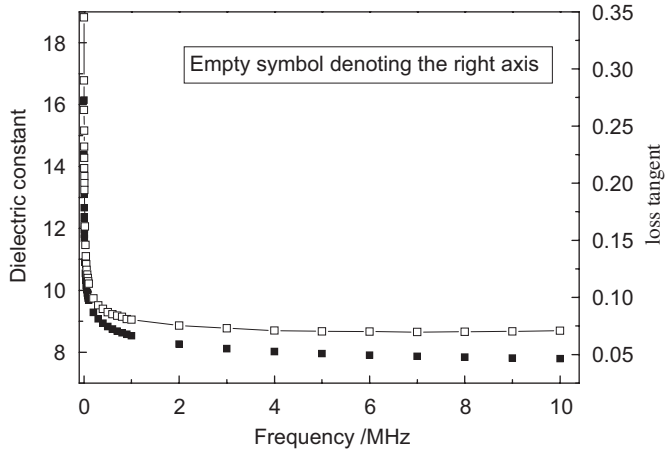

Fig. 3. Room temperature frequency dependence of dielectric constant and dielectric loss for freestanding diamond film.

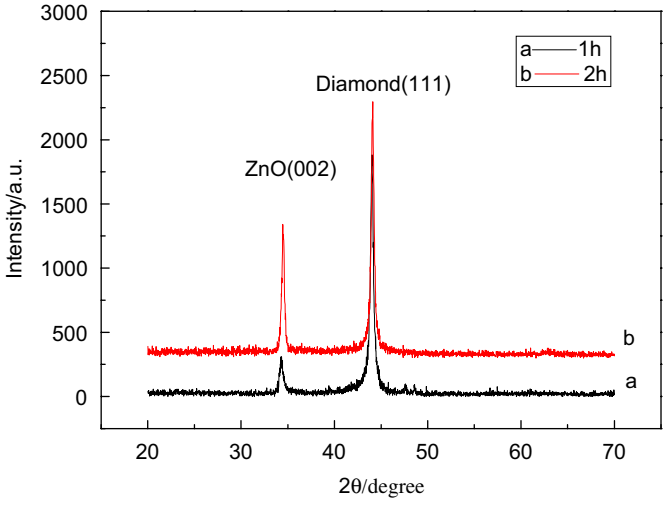

Fig. 5. XRD patterns for ZnO films on diamond film substrates for different sputtering time.

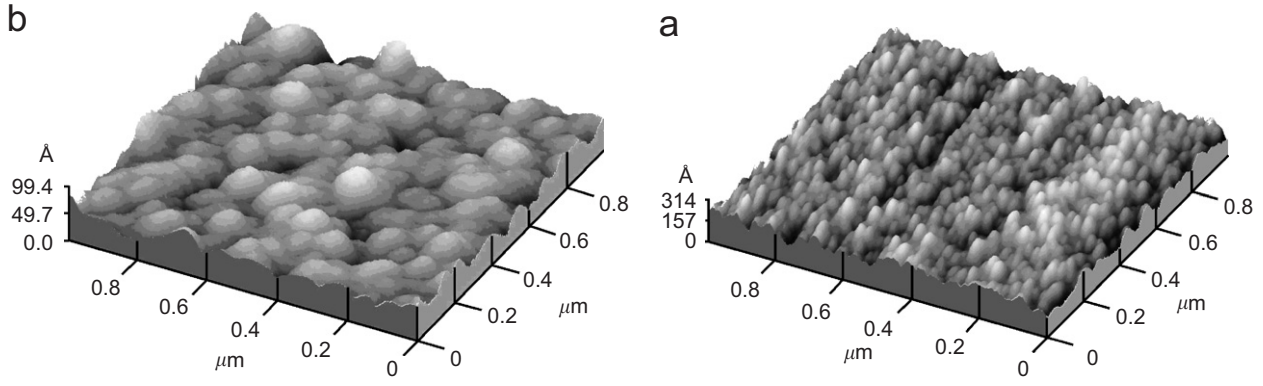

Fig. 4. AFM images for ZnO films on diamond film substrates for different sputtering times: (a) 1 h and (b) 2 h.

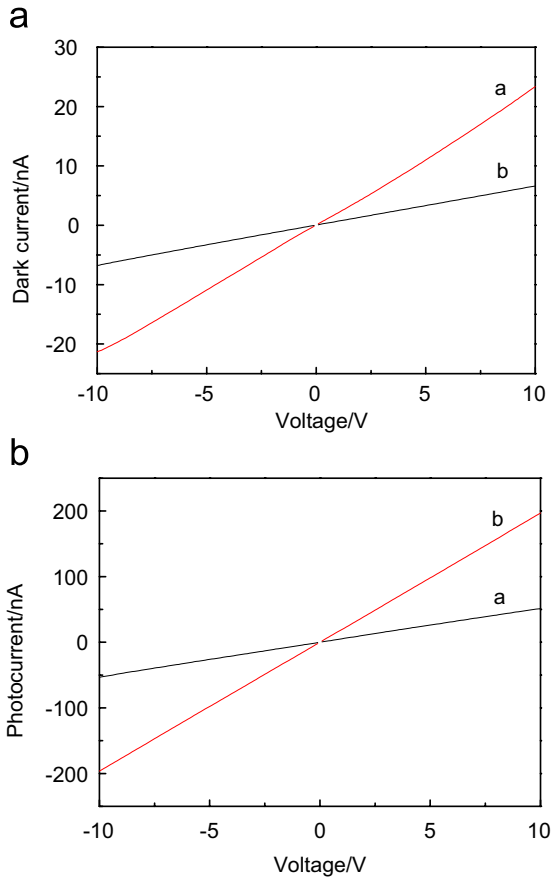

Fig. 6. (a) The dark current and (b) the photocurrent voltage characteristics for ZnO/diamond film structure photodetectors.

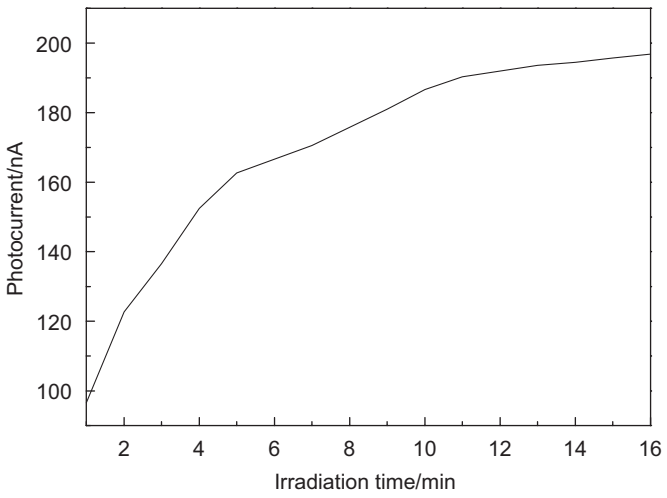

Fig. 7. The time-dependent photocurrents of the photodetector with UV-light irradiation.

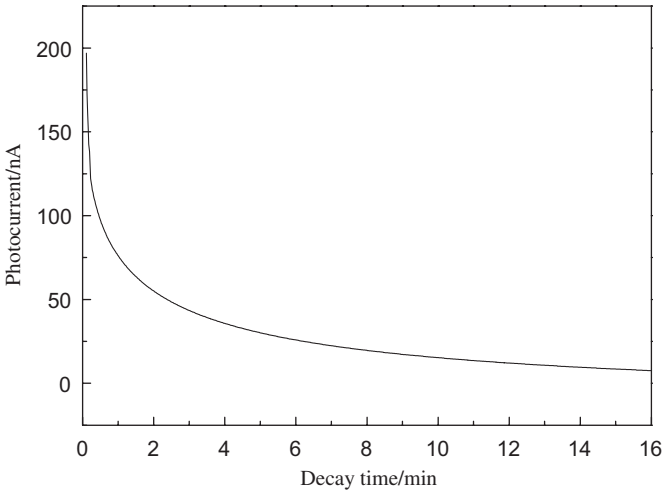

Fig. 8. The photocurrent decay characteristic of the photodetector without UV-light irradiation.

where q is the electron charge, F_0 the number of incident photons per unit time, η_{abs} the optical absorption efficiency, $\mu\tau$ the mobility-lifetime product of photo-generated carriers, d the interelectrode spacing and E is the applied electrical field.

The dark current is about 23.3 and 6.6 nA, and the photocurrent is about 51.4 and 196.8 nA under a bias voltage of 10 V for samples a and b. Usually, when ZnO films are irradiated by UV light, free carriers (electron–hole pairs) are generated, which under external electric field, move towards electrodes. The difference between the detector a and the detector b may be due to the different film microstructures. Because grain boundaries are full of traps (defects or impurities), which would capture free carriers, the film b has bigger grain size, which means that there exists much less grain boundaries in the film b than in the film a with smaller grain size. Obviously, with the increase of grain size, the dark-current decreases and the photocurrent increases.

The $\mu\tau$ value can be estimated from Eq. (4) of about $10^{-7}\,cm^2/V$ for the photodetector b.

Fig. 7 shows a time-dependent photocurrent characteristic for photodetector b under a bias voltage of 10 V. The photocurrent increases swiftly and then saturates gradually with the irradiation time process. The polycrystalline nature of ZnO film is responsible for the trapping centers that can seize the carriers before moving apart and being collected by electrodes. Initially, there exist a large number of trapping centers which are filled slowly by the carriers generated by UV light, leading to the increase in photocurrent with irradiation time. After a certain time (about 10 min), the effective number of trapping centers is in equilibrium, i.e. the carriers produced can almost be collected, and therefore the photocurrent tends to reach saturation. This carrier trapping effect was also named the polarization effect [16].

Fig. 8 shows photoresponse decay process for photo-detector b under a bias voltage of 10 V. It takes more than 3 min for the photocurrent to drop to 20% of the maximum value. We attribute this process to a large number of trapping centers capturing the photo-generated

carriers, which reduces the probability for carriers recombining and prolongs the photocurrent decay time.

Due to using the polycrystalline ZnO films with high densities of grain boundaries which are full of traps, the MSM photoconductor shows the transient UV response with a long photocurrent rise and decay time of around 10 and 3 min, respectively. In order to improve the photoresponse speed, we think, high-quality ZnO film with large grain size or its single-crystal material should be used. In addition, the high-speed photodetector can also be fabricated with p–n junction.

4. Summary

Highly *c*-axis-oriented ZnO thin films with different grain sizes were deposited on the freestanding diamond films by RF reactive magnetron sputtering. A dielectric constant of 7.78 and dielectric loss 0.07 at a frequency of 10 MHz for freestanding diamond film were acquired. The strong increase in the dielectric constant and the dielectric loss at low frequencies was due to an LFD.

I–V characteristics of UV photodetectors with ZnO/diamond structure were studied and a significant photoresponse was observed under UV light illumination. The dark current, photocurrent voltage characteristics appeared nearly symmetric and linear, suggesting that a fine ohmic contact was formed. The dark current and the photocurrent of the ZnO photodetectors were relative to the grain size and the quality of ZnO films. For the photodetector with a bigger grain size, a weaker dark current of 6.6 nA and a stronger photocurrent of 196.8 nA were obtained under10 V bias voltage.

The photocurrent rise and decay process confirmed the carrier trapping effect.

Acknowledgments

This work was supported by the National Natural Science Foundation of China under Grant No. 60577040, the Shanghai Foundation of Applied Materials Research and Development (0404), Nano-technology projects of Shanghai (No. 0452nm051, 0552nm046) and Shanghai Leading Academic Disciplines (T0101).

References

[1] P.W. May, Philos. Trans. R. Soc. Lond. A 358 (2000) 473.
[2] S.T. Lee, Z. Lin, X. Jiang, Mater. Sci. Eng. 25 (1999) 123.
[3] Q.F. Su, J.M. Liu, L.J. Wang, et al., Scripta. Mater. 54 (2006) 1871.
[4] L.H. Shu, A. Christou, D.F. Barbe, Microelectron. Reliab. 36 (1996) 1177.
[5] S.J. Pearton, D.P. Norton, K. Ip, Y.W. Heo, T. Steiner, Superlattice. Microstruct. 34 (2003) 3.
[6] W. Gao, Z. Li, Ceram. Int. 30 (2004) 1155.
[7] Q.A. Xu, J.W. Zhang, K.R. Ju, X.D. Yang, X. Hou, J. Crystal Growth 289 (2006) 44.
[8] C.X. Wang, G.W. Yang, C.X. Gao, et al., Carbon 42 (2004) 317.
[9] D. Basak, G. Amin, B. Mallik, et al., J. Crystal Growth 256 (2003) 73.
[10] J.M. Liu, Y.B. Xia, L.J. Wang, et al., Trans. Nonferrous Meta Soc. China 16 (2006) s298.
[11] M. Silveira, M. Becucci, E. Castellucci, et al., Diam. Relat. Mater. 9 (1993) 1257.
[12] I.W. Kim, D.S. Lee, S.H. Kang, et al., Thin Solid Films 441 (2003) 115.
[13] S. Selvasekarapandian, M. Vijayakumar, Solid State Ionics 148 (2002) 329.
[14] J.B. Lee, M.H. Lee, C.K. Park, J.S. Park, Thin Solid Films 447 (2004) 296.
[15] S. Salvatori, E. Pace, M.C. Rossi, et al., Diam. Relat. Mater. 6 (1997) 361.
[16] E.K. Souw, R.J. Meilunas, Nucl. Instr. Meth. A 400 (1997) 69.